Probability and output analysis of asymmetric bistable energy harvesters driven by Gaussian white noise

Wei Wang[1], Junyi Cao[1, a], Chris R. Bowen[2], Grzegorz Litak[3, 4]

[1]Key Laboratory of Education Ministry for Modern Design and Rotor-Bearing System, School of Mechanical Engineering, Xi'an Jiaotong University, Xi'an, Shaanxi, 710049, China

[2]Materials and Structures Centre, Department of Mechanical Engineering, University of Bath, Bath, BA27AY, UK

[3]Faculty of Mechanical Engineering, Lublin University of Technology, Nadbystrzycka 36, Lublin 20-618, Poland

[4]Department of Process Control, AGH University of Science and Technology, Mickiewicza 30, 30-059 Krakow, Poland

Abstract.

Due to their excellent broadband response and high sensitivity to low amplitude excitations, there is significant interest in the theoretical analysis and experimental validation of bistable energy harvesters (BEHs). However, in practice it is difficult to obtain a perfectly symmetric bistable potential function, and our current understanding of the influence of asymmetric functions on the response of BEHs is limited. As a result, this paper sheds new light on the influence of asymmetric potentials on the response probability and harvested electrical outputs of BEHs driven by Gaussian white noise. Firstly, the influence of potential well depth on the power outputs and response probability of symmetric BEHs is illustrated. When a quadratic nonlinearity is introduced to characterize the asymmetry, numerical simulations demonstrate that it has a negative effect on the

[a]Electronic mail:caojy@mail.xjtu.edu.cn

output of a BEH under relatively low amplitude excitation and the negative influence becomes greate with an increase of the degree asymmetry. Using probability analysis, it is indicated that the probability density function of displacement strongly depends on the degree of asymmetry of the potential functions and it is also affected by the excitation intensity. Finally, experiments are carried out which demonstrate that the average output power is indeed influenced by the asymmetric potential of the BEHs under different excitation levels.

Keywords: Energy harvesting; Bistable; Asymmetric potential; Gaussian white noise; Probability

1. Introduction

In the last few decades, the fast-growing market for wireless sensors and portable electronics has motivated an increasing and insistent demand for small-scale energy supply technologies which are environmentally friendly[1]. As an alternative approach to provding power, the technology of energy harvesting has garnered a great deal of attention from all over the world due to it promising perspective of being able to supply electricity for low-power consumption devices[2-4]. The core of energy harvesting is the ability to convert wasted energy in the environment, such as ambient vibrations[5], human-body motion[6] and heat, into useful electrical energy using piezoelectric[7,8], electromagnetic[9,10] and thermoelectric[11,12] type approaches. Among the various energy conversion mechanisms, piezoelectric-based configurations are viewed as a promising solution for their high energy density and ease of fabrication[13,14]. Previously, linear piezoelectric energy harvesters based on traditional linear resonance mechanism have been designed and optimized with a variety of materials and structures[15]. However, the performance of linear harvesters that operate at a fixed resonant frequency is greatly reduced when it is subjected to ambient vibrations with a wide frequency range[16,17].

To address this problem, approaches based on mechanical[18] and nonlinear[19,20] mechanisms to enhance the energy harvesting performance by increasing the operating frequency bandwidth have been widely investigated[21]. In particular, nonlinear multi-stable energy harvesting configurations with different types of potential distributions have been theoretically analyzed and experimentally validated. For instance, Zhang et al.[22] presented a novel piezoelectric energy harvesting device based on a nonlinear energy sink. Song et al.[23] demonstrated a broadband energy harvester array by coupling each harvester in an array through the interaction of magnetic proof masses. More

recently, Fan et al.[24] proposed a piezoelectric energy harvester with stoppers which made the device monostable to harvest energy from harmonic and random vibrations.

Because of their high sensitivity to low excitation levels, bistable energy harvesters (BEHs) with double potential wells have received significant interest. In terms of the configurations of the BEHs employed, Erturk et al.[25,26] introduced a bistable piezomagnetoelastic device for enhancing energy harvesting performance under broadband random excitations. Masana et al.[27] developed a BEH using axially loaded beams and provided a comprehensive understanding of it mode of operation. Arrieta et al.[28] presented a piezoelectric bistable composite for broadband energy harvesting, revealing its wide bandwidth operation of high power conversion. Furthermore, Zhou et al.[29] reported a BEH that coupled end magnets with two rotatable external magnets and demonstated its improved performance compared with a linear harvester. Liu et al.[30] investigated the inter-well motion of a buckled-spring-mass generator by applying the harmonic balance method, providing some significant results regarding a parameter optimization study. More recently, Wolszczak et al.[31] considered a bistable flexible beam that moved as an inverted pendulum between amplitude limiters. In order to further understand the impact of the range of potential functions, additional energy harvesters are being developed based on tristable[32], quad-stable[33] and penta-stable[34] configurations to collect energy from broader and lower intensity vibrations.

In terms of nonlinear multi-stable energy harvesters, a number of researchers have focused on investigating their nonlinear response characteristics when subjected to random excitations. For example, Litak et al.[35] numerically considered the response of a BEH driven by stationary Gaussian white noise. Daqaq[16] solved the Fokker-Plank-Kolmogorov (FPK) equation for the probability density function (PDF) of an inductive bistable generator in the white noise limit,

concluding that bistabilities in the potential function provide no enhancement over a traditional linear system. Later, he applied the same theory to a piezoelectric BEH subjected to white Gaussian excitations and demonstrated the BEH can only outperform the linear system when designed with the appropriate potential energy function[17]. Yang et al.[36] investigated the response of a monostable harvester with a fractional derivative damping under Gaussian white noise excitation using the method of stochastic averaging. In addition, Jiang et al.[37] applied the same method by using the generalized harmonic functions to analyze different types of Duffing vibration energy harvesters under Gaussian white noise excitation. As an effective method to improve the performance under a random excitation, the concept of stochastic resonance was applied to the field of energy harvesting. As an example, the stochastic resonance of bistable harvesters was investigated by Zheng et al.[38] and it was indicated that the harvested power under stochastic resonance was noticeably higher than that other conditions. Li et al.[39] considered a BEH driven by a harmonic axial load and transverse random excitations. Stochastic resonance was observed in their system and the occurrence condition was derived by a Kramers escape rate. Additionally, the stochastic resonance of a tristable electromechanical coupled harvester was exploited by Jin et al.[40]. Furthermore, coherence resonance is viewed as a special case of stochastic resonance[41], and this phenomenon has been intensively investigated by the group of Qin[42,43].

Based on this work to date, it is emphasized that the majority the research described above is based on multi-stable energy harvesters with perfectly symmetric potential energy functions. However, in practice it is difficult to fabricate a nonlinear system with a completely symmetric potential function due to material and structural impefections, or due to the impact of gravity. This bringing new concerns for developing a better understanding of the essential physical scientific

problems associate with asymmetric potential functions in such systems. In terms of previous work, Badzey et al.[44] observed an asymmetric potential in a bistable nanomechanical oscillator. Chizhevsky et al.[45] experimentally studied the phenomenon of vibrational resonance in an asymmetric bistable system with agreement between analytical and numerical results. Jeyakumari et al.[46] analyzed how the asymmetry in potentials influence the vibrational resonance of a Duffing oscillator and Cveticanin et al.[47] indicated that the motion of an asymmetric oscillator can be periodic but also unbounded and depends on the relation between the parameters of the system and its initial position. In the specific area of energy harvesting, Harne and Wang[48] considered the influence of asymmetry due to a bias angle on the performance of monostable and bistable harvesters driven by colored noise. He and Daqaq[49] investigated the effect of an asymmetric quadratic nonlinearity[50] on nonlinear energy harvesters and showed that the output of a monostable harvester increases with the degree of potential function asymmetry, while the influence is opposite for a BEH system. Additionally, Wang at al.[51] investigated the influence of asymmetric potentials in bistable harvesters and proposed a method to eliminate the negative effect and they also demonstrated that an asymmetric BEH could operate constructively with the asymmetric motion of a human lower limb to improve the output power from a human body[52]. Zhou et al.[53] theoretically deduced the harmonic balance solutions of asymmetric tristable energy harvesters, and their analysis showed that the potential barrier is a significant factor to determine the orbit height of high-energy inter-well oscillations. More recently, Li and Zhou[54] presented a probability analysis of an asymmetric tristable harvester based on Monte Carlo simulations. Although much effort has been devoted to the study of asymmetric nonlinear energy harvesters, the detailed investigation into the probability and power outputs of asymmetric BEHs driven by Gaussian white noise is still an open

issue to be explored.

Therefore, this paper focuses on the influence of asymmetry on the response probability and power outputs of asymmetric BEHs excited by Gaussian white noise. The paper is organized as follows: Section 2 illustrates the configuration of the asymmetric potential BEH and the development of the corresponding dynamic model. In Section 3, the influence of potential well depth on the output power and probability of symmetric BEHs is numerically considered. In particular, the influence mechanism of asymmetric potentials is also presented based on output voltage and probability density function (PDF). In Section 4, experimental results are presented and the conclusion is summarized in Section 5.

2. Illustration of configuration and dynamic model

A schematic diagram of the nonlinear magnetic coupling BEH is illustrated in Fig. 1. The system is composed of a stainless steel beam, two symmetric PZT-51 piezoelectric layers pasted at the root, two tip magnet attachments and two external rotary magnets. By adjusting the appropraite parameters of d, h, and ϑ, the system can be made to achieve a bistable configuration. Due to the existence of imperfections in the structure and materials, real bistable systems will exhibit an asymmetric potential energy functions. Without external magnets, the system becomes a linear harvester. In this condition, the variational indicator (V^I) should always be zero through the Lagrange function, as shown in the following:

$$V^I = \int_{t_t}^{t_2} \left[\delta E_{\mathrm{k}} - \delta E_{\mathrm{p}} + E_{\mathrm{a}} \right] d\bar{t} = 0 \tag{1}$$

where δ is the variational symbol and E_{k}, E_{p} and E_{a} are the kinetic energy, potential energy, and the external work applied to the system respectively. Based on the Euler-Bernoulli beam theory and Rayleigh-Ritz method, the dynamic model of the linear harvester under base excitation could be

expressed as

$$\begin{cases} m\ddot{r} + c\dot{r} + kr - \theta\bar{V} = F(\bar{t}) \\ C_p\dot{\bar{V}} + \bar{V}/R + \theta\dot{r} = 0 \end{cases} \tag{2}$$

in which m, c, k and θ are respectively the equivalent mass, damping, stiffness, and electromechanical coupling coefficient. C_p and R represent the equivalent capacitance of the piezoelectric and external load resistance. In addition, r is the tip displacement of the cantilever, $\bar{V}$ is the voltage output and F is the external excitation. For a nonlinear system, the linear force in Eq. (2) is replaced by $d\bar{U}(r)/dr$, where $\bar{U}(r)$ represents the potential energy function.

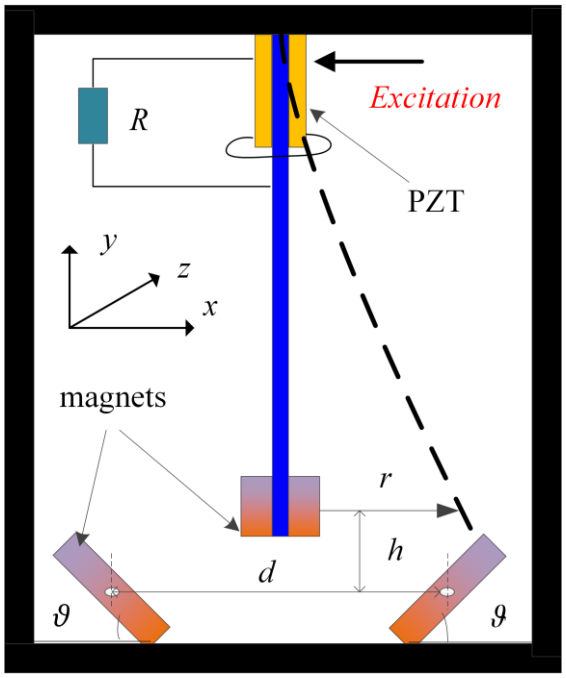

Fig. 1. Schematic diagram of the asymmetric potential bistable energy harvester (BEH).

For brevity, the dynamic model is nondimensionalized in the following simulation, and the corresponding model for an asymmetric potential BEH[51,55] under Gaussian white noise is

$$\begin{cases} \ddot{x} + 2\xi\dot{x} - x + \beta x^2 + \delta x^3 - \kappa^2 V = n(t) \\ \dot{V} + \alpha V + \dot{x} = 0 \end{cases} \tag{3}$$

where x, v and t are, respectively, the nondimensional displacement, voltage, and time, and ξ is the damping ratio. β and δ are the coefficient of the quadratic and cubic nonlinearities. In addition,

κ^2 is the dimensionless electromechanical coupling coefficient, and α is the ratio between the mechanical and electrical time constants. In the equation, $n(t)$ can be depicted as $\sqrt{2D}\varsigma(t)$, in which D represents the noise intensity and $\varsigma(t)$ is Gaussian white noise with a mean value and variance equaling to 0 and 1. For the nondimensionalized model, the potential energy function of the system is

$$U(x) = -\frac{1}{2}x^2 + \frac{1}{3}\beta x^3 + \frac{1}{4}\delta x^4 \tag{4}$$

When β equals to zero in Eq.(4)~~(4)~~, the symmetric BEH has one unstable equilibrium point $x_m = 0$ and two stable equilibrium point $x_n = \pm\sqrt{1/\delta}$, and the potential well depth is shown as

$$\Delta U = \frac{1}{4\delta} \tag{5}.$$

3. Numerical simulation

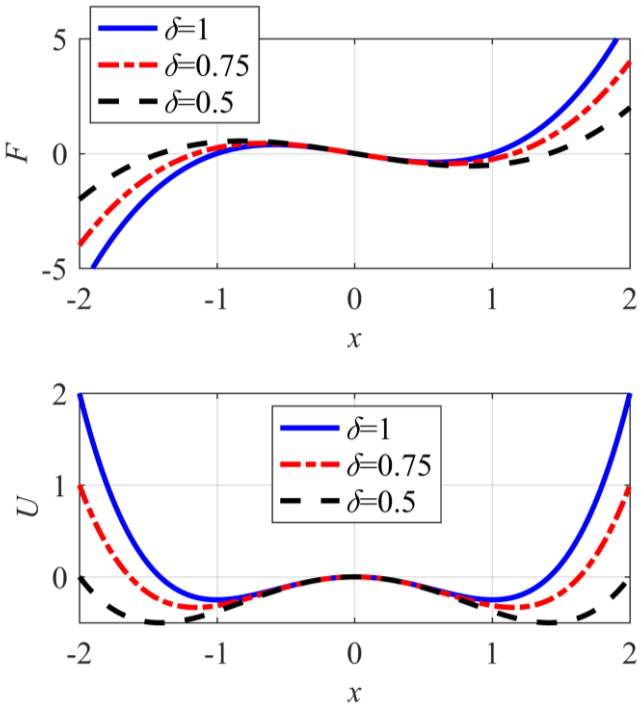

Fig. 2. Restoring forces and potential energy functions for δ=1 , 0.75 and 0.5 when β equals to 1.

In this section, numerical simulations are carried out to investigate the influence of asymmetric potentials on response probability and power outputs of BEHs, and a fourth-order Runge-Kutta

algorithm is applied to obtain the numerical solutions of the model. Before we report the study into asymmetric potentials, the potential well depth of a symmetric BEH is considered by comparing the electric output and the PDF of displacement. In addition, the Kramers escape rate is provided to illustrate the numerical results. Thereafter, the influence of asymmetric potentials is investigated based on the harvester electric output and PDF. It is worth highlighting at this stage that the electric outputs are obtained by averaging 10 independent simulations, while a 1000 simulations are examined for the PDF.

3.1 Influence of potential well depth

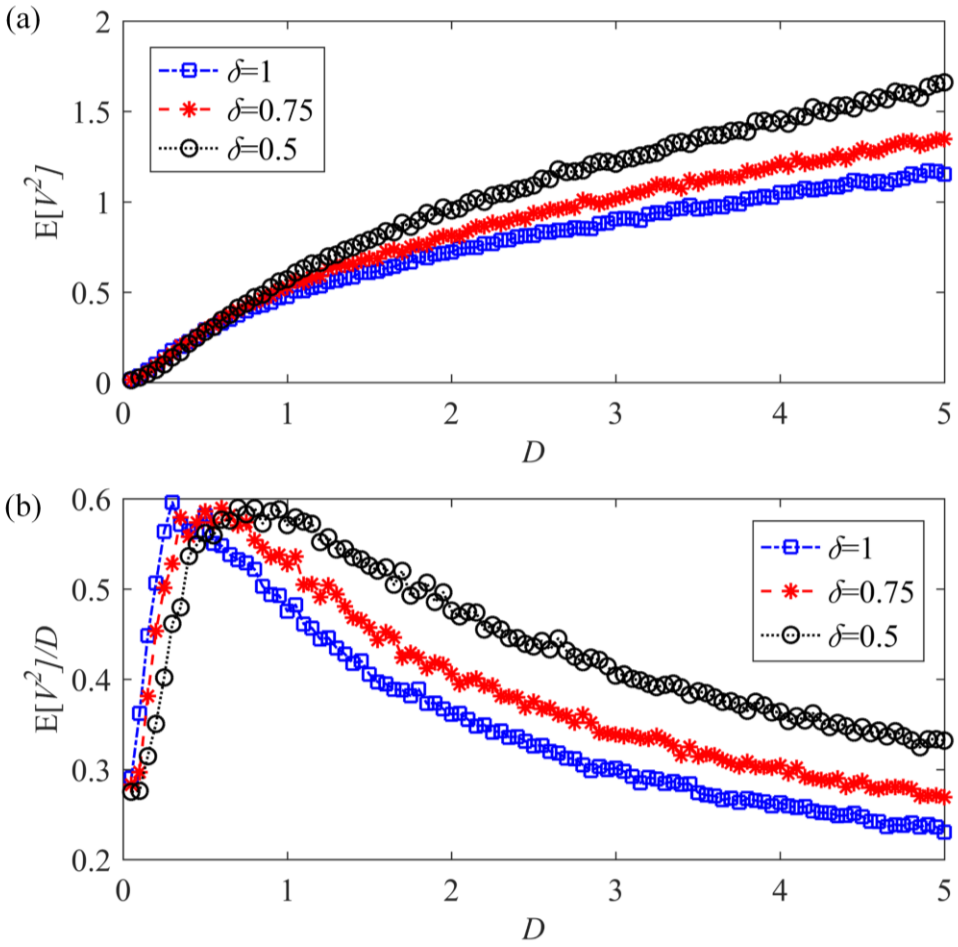

Fig. 3. Relationship between the system's response and excitation level for different values of δ : (a) the mean square value of voltage; (b) the ratio of mean square value of voltage to excitation level.

In the investigation into the influence of the potential well depth on the probability and output

response of symmetric BEHs, parameters in Eq.(4)~~(4)~~ are considered with δ=1, 0.75 and 0.5 for β equaling to 0. Figure 2 (a) and (b) show the nonlinear restoring forces and potential energy functions respectively of the three BEHs with different potential well depths. It is seen that the potential well depth of the BEH increase with a decrease in the value of δ and the maximum potential well depth reaches 0.5 when δ equals to 0.5. Additionally, it is noticed that when the potential well depth increases, the distance between the two wells becomes larger.

In the simulation, the mean square value of output voltage $E[V^2]$, and the ratio of $E[V^2]$ to excitation intensity D are applied to compare harvesting performance. In Fig. 3 (a), the relationship between $E[V^2]$ and excitation intensity is shown and it can be seen that $E[V^2]$ increases with an increase in the excitation intensity for the BEHs with any potential well depth. With regard to the output at a specific excitation level, the BEH with a shallower potential well has a larger value for $E[V^2]$ at a low excitation intensity. When the excitation intensity increases over a certain value, $E[V^2]$ will have a larger value for a BEH with a deeper potential well. The reason for this phenomenon can be explained that when the excitation intensity is low, the oscillation of the BEH is limited to a single potential well and the output mainly depends on the potential well depth. However, when subjected to a relatively large excitation level, the BEH travels across the potential barrier and the distance between the two potential wells contributes a larger electrical output. Therefore, it is seen from Fig. 3 (b) that the ratio of $E[V^2]$ to excitation intensity of a BEH with a shallower potential well has a larger value for a realively low excitation intensity while a smaller one for large excitation level. Overall, the ratio of $E[V^2]$ to excitation intensity firstly increases rapidly with an increase of excitation intensity, and then decreases when the excitation intensity increases over a critical value. The critical excitation intensity mainly depends on the potential well depth of the BEH and has a larger value for

BEH with deeper potential wells.

For a symmetric potential BEH with δ equaling to 1, we present several special cases for excitation intensity of 0.1, 0.3 and 0.5 to investigate the nonlinear dynamics of the system. Figure 4 (a) shows the time history of the system's displacement for a noise intensity of 0.1. In this condition, the system occasionally travels across the potential barrier and generates a larger voltage output, although the oscillation of the BEH is limited to a sinlge potential well for the majority of the time. This behaviour can also be seen by the corresponding phase diagram, illustrated in Fig. 4(a), in which there are only several trajectories across the potential well. When the excitation intensity is increased to 0.3, the time history of the displacement and corresponding phase trajectory are seen explained in Fig. 4(b) which indicates that the system travels across the potential barrier more frequently, and the maximum value of displacement response also increases when compared with the results in Fig. 4(a). As the noise intensity is further increased to 0.5, more significant performance enhancements can be observed in Fig. 4(c). In general, the system is more likely to achieve inter-well oscillation and output larger electrical power with an increase in the excitation intensity.

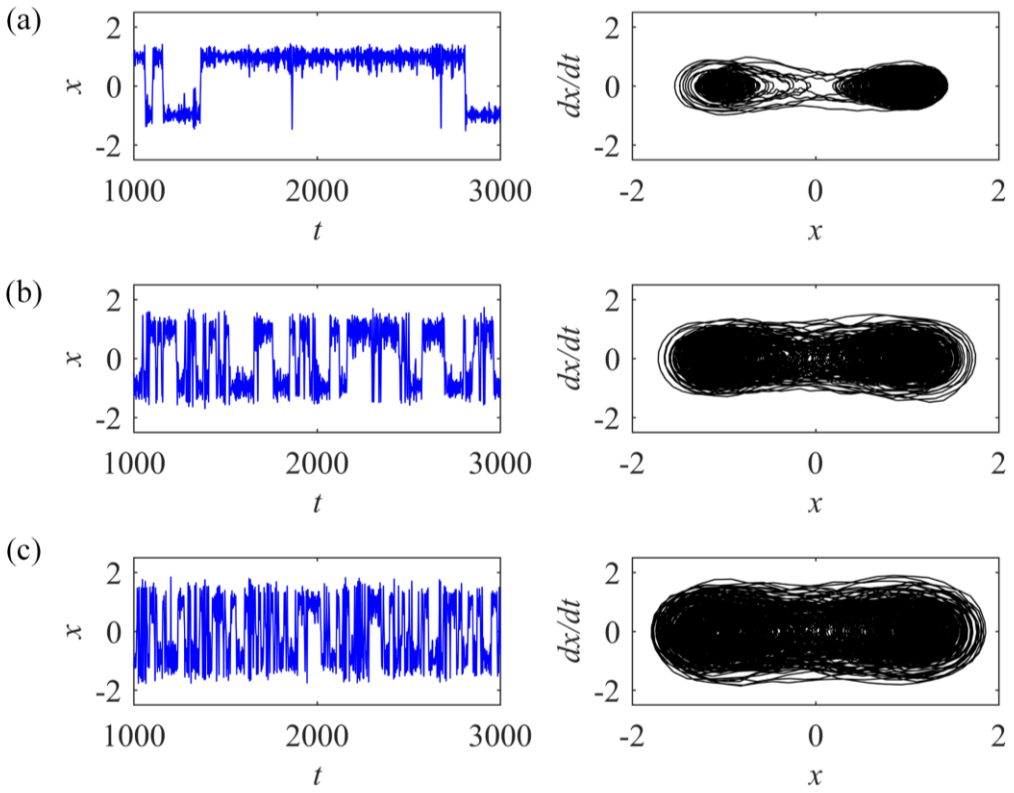

Fig. 4. Time history of the system's displacement and corresponding phase trajectory for β=0 and δ=1 under different excitation level: (a) D=0.1; (b) D=0.3; (c) D=0.5.

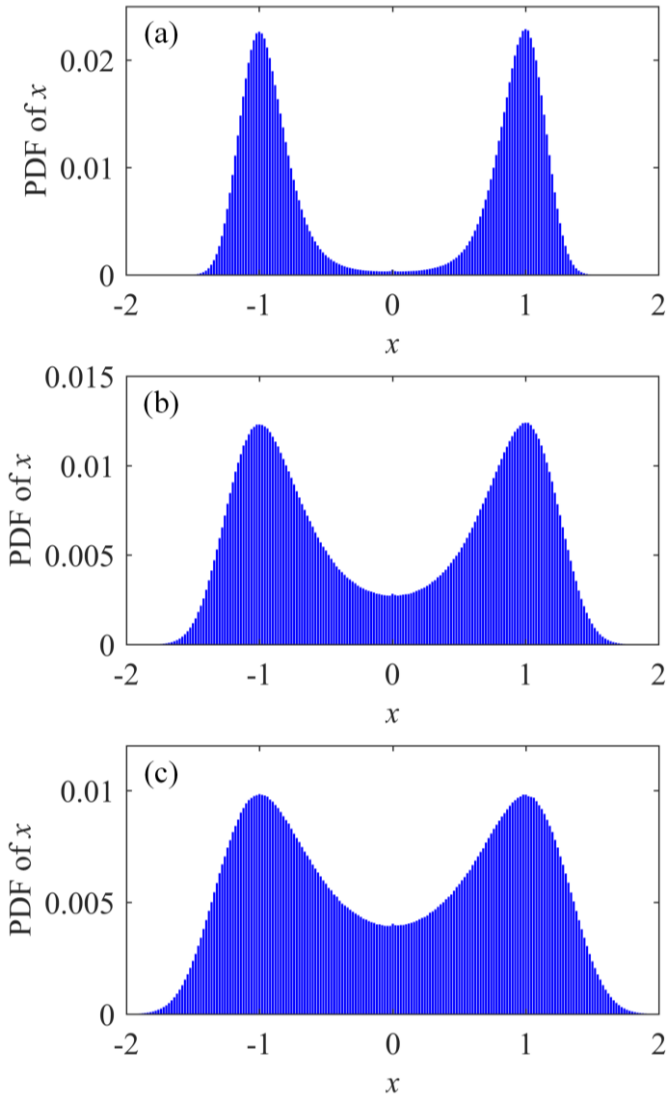

Fig. 5. Probability density function of x under different excitation level: (a) D=0.1; (b) D=0.3; (c) D=0.5.

For the three cases in Fig. 4, the simulations for each excitation level are undertaken for 1000 times to obtain the PDF of displacement. One point that should be emphasized here is that the initial displacement in the simulation is set to zero so that the oscillator can reach each potential well with the same probability when there is no efficient energy for the system to undertake inter-well motion at the beginning. Figure 5 (a) shows the PDF of displacement for a low noise intensity of 0.1. A distinct bimodal distribution is obtained and shows that the system has a larger probability to oscillate in the two potential wells. For a larger noise intensity of 0.3, the PDF in Fig. 5 (b) has a

smaller probability around the two potential wells and a larger one around the potential barrier, demonstrating that more inter-well motion is achieved compared with the condition in Fig. 5 (a). As the noise intensity further increased to 0.5, more frequent inter-well oscillation is obtained with a larger probability of displacement around the potential barrier shown in Fig. 5 (c); these results and observations are consistent with that in Fig. 4.

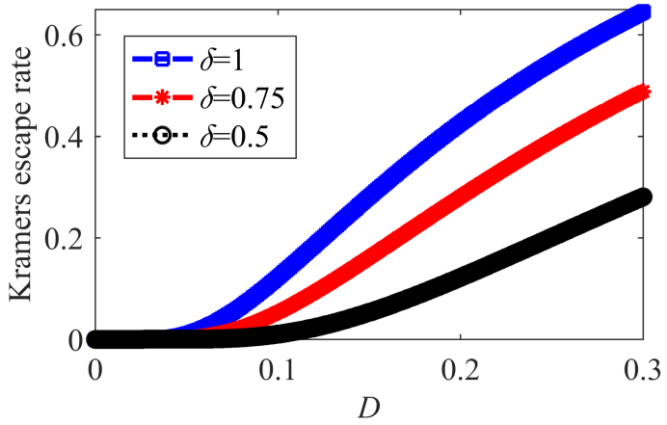

Fig. 6. Kramers escape rates for δ equaling to 1, 0.75 and 0.5.

To explain the phenomenon shown in Fig. 4 and 5, the Kramers escape rate is presented to qualitatively describe the hopping between two potential wells of the BEH. For a typical bistable system, the Kramers escape rate[56,57] is defined as

$$r_K = \frac{\omega_m \omega_n}{2\pi \cdot 2\xi} \exp(-\frac{\Delta U}{D}) \tag{6}$$

where $\omega_m = \sqrt{U''(x_m)}$ and $\omega_n = \sqrt{U''(x_n)}$ are the vibrational angular frequency at the unstable and stable equilibrium point respectively. Substituting Eq.(5)~~(5)~~ into Eq.(6)~~(6)~~, the Kramers escape rate of the BEH investigated is expressed by following.

$$r_K = \frac{1}{\sqrt{2}\pi \cdot 2\xi} \exp(-\frac{1}{4\delta D}) \tag{7}$$

For the BEHs with different potential well depth investigated above, the corresponding Kramers escape rate are respectively shown in Fig. 6 for δ equaling to 1, 0.75 and 0.5. For a BEH with a

specific potential well depth, there is a critical excitation intensity. When the excitation intensity is lower than the critical value, the Kramers escape rate is close to zero indicating that the probability to achieve inter-well motion is low. However, the Kramers escape rate increases rapidly when the noise intensity is above the critical value, which indicates that the BEH has a larger probability to cross the potential barrier. The change in the PDF of displacement shown from Fig. 5 (a) to (c) could be explained by the variation of the Kramers escape rate. Under a specific excitation level, it is seen that a BEH with deeper potential wells has a smaller value of the Kramers escape rate. This change indicated that an increase of potential well depth will increase the probability of the BEH to oscillate within a potential well, while a smaller well depth leads to increased probability to travel across the potential barrier. The change in the PDF of displacement for BEHs with δ equaling to 0.75 and 0.5 under an excitation intensity of 0.3 is shown in in Fig. 7 (a) and (b) clarify the variation in Kramers escape rate perfectly.

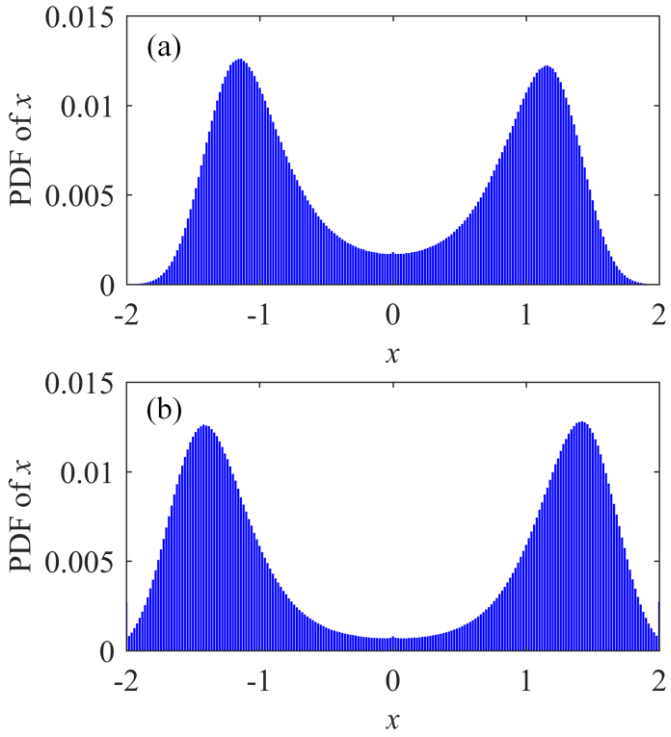

Fig. 7. Probability density function of x at D=0.3 and β=0 : (a) δ =0.75; (b) δ =0.5.

3.2 Influence of asymmetric potential energy functions

To investigate the influence of asymmetric potentials on the response probability and electrical outputs, three asymmetric BEHs are considered here with β equaling to 0.20, 0.35 and 0.5 when the coefficient of cubic nonlinearity is 1. The nonlinear restoring forces and potential energy functions of the three asymmetric BEHs are illustrated in Fig. 8, along with a symmetric function for comparison where $\beta=0$. From Fig. 8, it is seen that the depth of the potential well on the left becomes larger, while the depth of the right one becomes smaller with an increase of the quadratic nonlinearity.

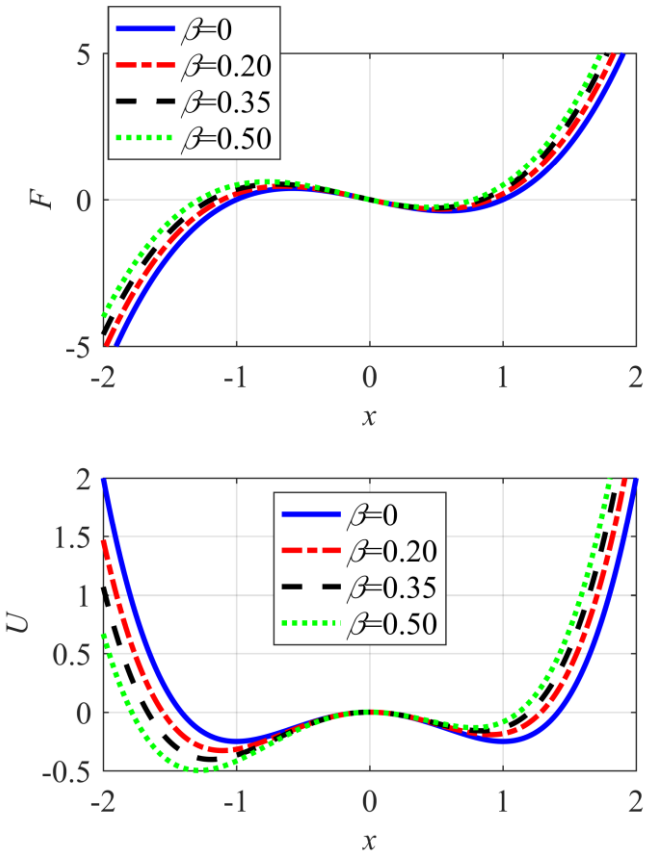

Fig. 8. Restoring forces and potential energy functions for β=0 , 0.2, 0.35 and 0.5 when δ =1.

Figure 9 (a) describes the mean square value of output voltage $E[V^2]$ for three asymmetric potential BEHs under different excitation intensities. When the intensity is relatively low, the

asymmetry of the BEH has a negative effect on the output, where the electrical output power of the BEH decreases with an increase in excitation intensity. When the excitation intensity is relatively large, the asymmetric potential almost has no significant influence on the output and the output power will increase with the increase of excitation intensity. Figure 9 (b) illustrates the ratio of $E[V^2]$ to excitation intensity D of the asymmetric BEHs under different excitation levels. When subjected to a low excitation intensity, the ratio of $E[V^2]$ to D decreases with an increase in the value of β, which demonstrates the negative effect of asymmetry that is observed in Fig. 9 (a). Furthermore, it can be seen that a BEH with a large degree of asymmetry needs a larger excitation intensity to reach the maximum of the ratio of $E[V^2]$ to D. The reason for this phenomenon is due to that the larger degree of asymmetry will result in a deeper potential well compared with the system with a smaller asymmetric degree.

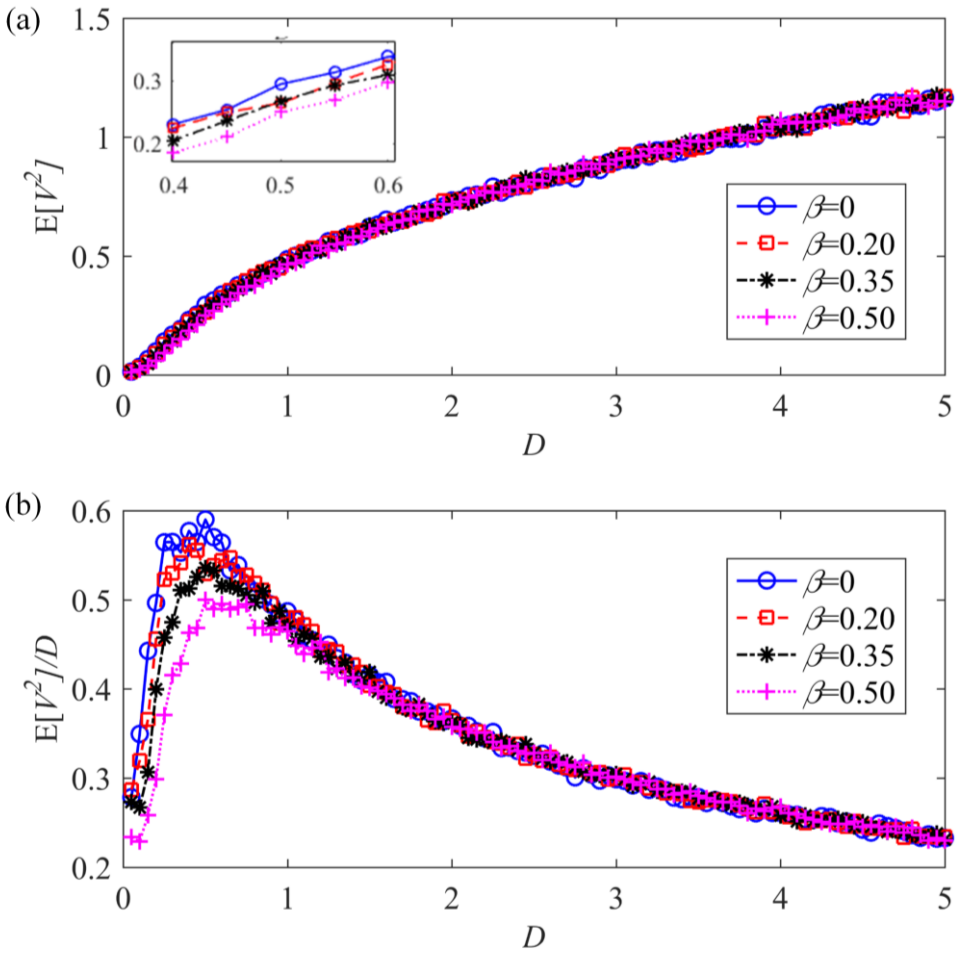

Fig. 9. Relationship between the system's response and the excitation level for different values of β: (a) the mean square value of voltage; (b) the ratio of mean square value of voltage to excitation level.

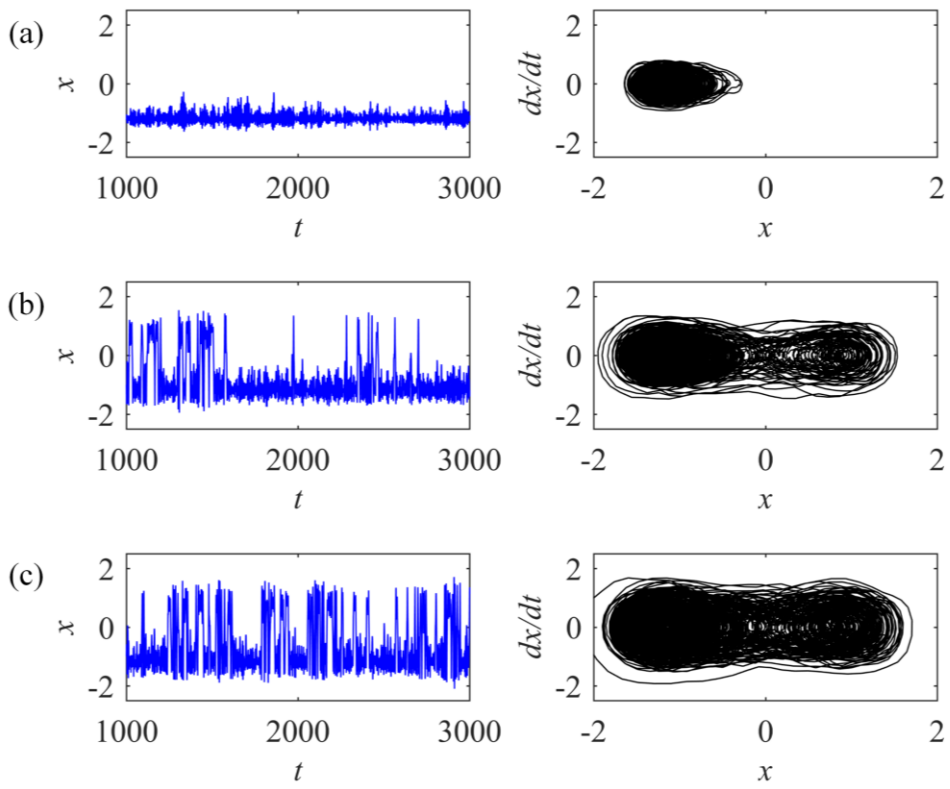

Fig. 10. Time history of the system's displacement and corresponding phase trajectory for β=0.35 at different excitation level: (a) D=0.1; (b) D=0.3; (c) D=0.5.

For β equaling to 0.35, the time history of the system's displacement and corresponding phase trajectory under a low excitation intensity of 0.1 are indicated in Fig. 10 (a). At a steady state, the oscillation of the system is always in the deeper potential well. As the excitation intensity increases to 0.3, the system is able to travel across the potential barrier chaotically and generate a larger power output, as shown in Fig. 10 (b). When there is no inter-well oscillation in this condition, the vibration of the system has a larger probability to stay in the deeper potential well. When the excitation intensity further increases to 0.5, the time history of displacement and phase trajectory in Fig. 10 (c) indicates that inter-well oscillation is achieved more frequently, thus generating a larger electrical output. Moreover, it should be stated that the maximum displacement obtained in the simulation will increase to larger values with an increase of noise intensity.

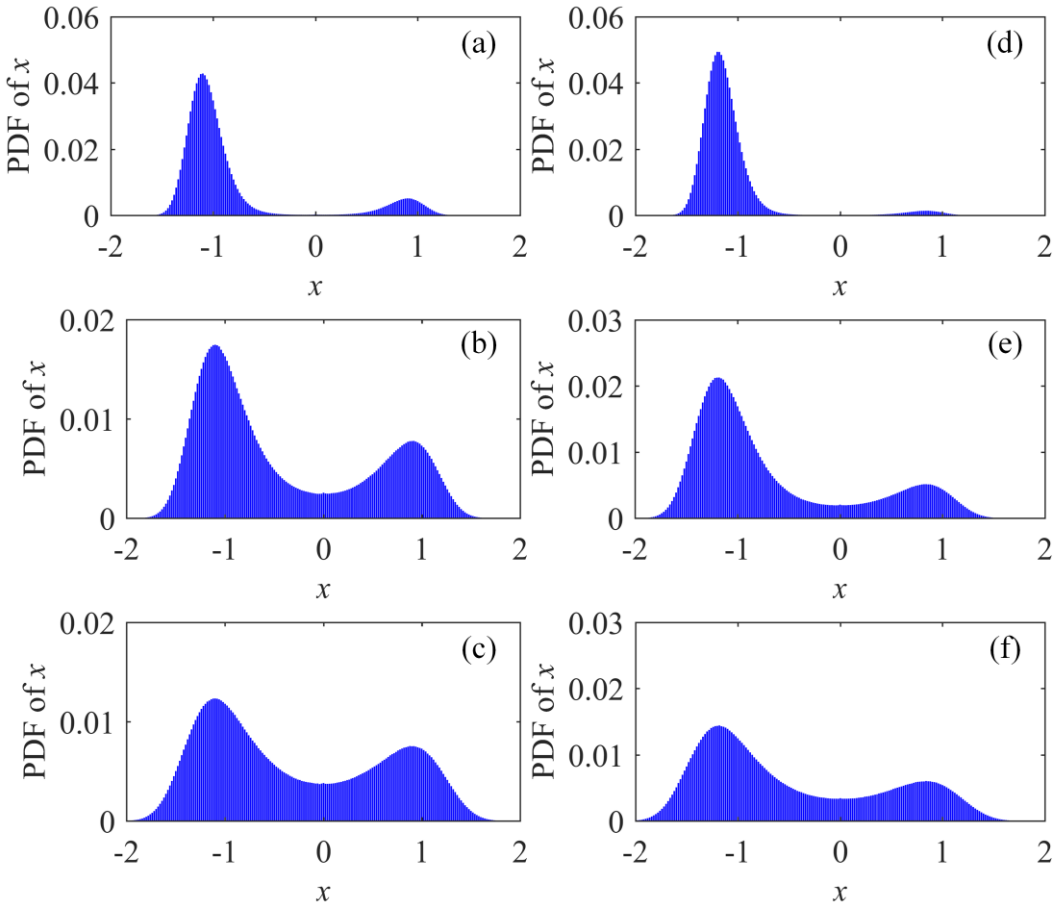

Fig. 11. Probability density function of x under different excitation level: (a) D=0.1, β=0.2; (b) D=0.3, β=0.2; (c) D=0.5, β=0.2; (d) D=0.1, β=0.35; (e) D=0.3, β=0.35; (f) D=0.5, β=0.35.

To better understand the response characteristics of asymmetric BEHs, the PDF of the displacement of the three asymmetric BEHs under excitation intensities of 0.1, 0.3, and 0.5 are now considered. To maintain the essential nature of the system, the initial displacement applied in the simulations is set to be 0 so that the oscillator can reach the two potential wells spontaneously depending on the different potential well depth when there is no efficient energy for the system to undertake inter-well motion at the beginning. For each situation, the numerical simulation is carried out 1000 times to calculate the PDF, and the PDFs of displacement for the system with β equaling to 0.2 under excitation intensity of 0.1, 0.3 and 0.5 are shown in Fig. 11 (a), (b) and (c) respectively. When the noise intensity is relatively low at 0.1, the shape of the PDF is almost unimodal in the

deeper potential well, showing that system has a large probability of oscillating in the deeper potential well while a smaller probability of oscillating in the shallower potential well. In addition, inter-well motion is limited under this excitation intensity. As the noise intensity increases, the PDF in Fig. 11 (b) and (c) a bimodal distribution is more apparent, but with asymmetrical shapes. This indicates that the system is able to achieve inter-well oscillations more frequently with an increase in the excitation intensity, while it is more likely to vibrate in the deeper potential well when the energy is insufficient for the system to cross the barrier. In general, the variation of the PDF discussed here is able explain the results and observations in Fig. 10.

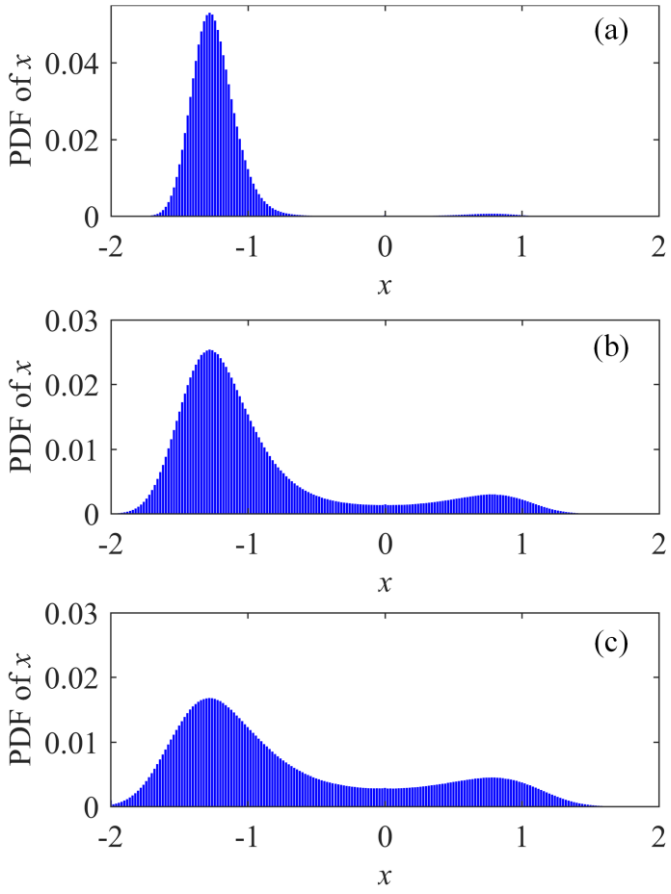

Fig. 12. Probability density function of x under different excitation level: (a) D=0.1, β=0.5; (b) D=0.3, β=0.5; (c) D=0.5, β=0.5.

The PDF of displacement for BEH with β equaling to 0.35 under excitation intensity of 0.1,

0.3 and 0.5 are shown in Fig. 11 (d), (e) and (f) respectively. The results in Fig. 11 (a), (b) and (c) shown that the asymmetric bimodal distribution becomes more obvious with an increase of noise intensity, indicating more inter-well motion is achieved. Under a certain excitation intensity, an increase of the degree to asymmetry makes the system have a smaller probability of oscillation across the potential barrier, thereby leading to greater oscillations in the deeper potential well. When the asymmetric degree increases with β equaling to 0.5, the PDF of displacement under different excitation intensity shown in Fig. 12 explains the influence of asymmetry on the response probability more clearly.

By comparing the numerical results of a BEH with an asymmetric potential with a BEH with a symmetric potential it is concluded that the asymmetry in the potentials has a negative influence on the electrical output and the effect will be aggravated with an increase in degree of asymmetry. From the probability analysis, the appearance of asymmetry makes the system have a larger probability to oscillate in the deeper potential well, thus resulting in the PDF exhibiting an asymmetric bimodal distribution depending on the asymmetric degree.

4. Experimental results and analysis

To verify the numerical simulations above, detailed experiments are carried out and two BEHs with different asymmetric potential energy functions were modulated in the experiment. The cantilever beam employed in this work was made form stainless steel with dimensions of 92×10×0.27 mm^3, with two piezoelectric layers at the root with dimensions of 12×10×0.8 mm^3. Figure 13 illustrates the potential energy functions of the two BEHs and it is seen that BEH-2 has deeper potential wells and a larger degree of asymmetry when compared with BEH-1. The BEHs were installed and exited with random excitations by a vibration exciter (JZK-50) which was controlled by

a signal generator (VT-9002-1) and a power amplifier (YE5874A). In the experiments, the vibrational frequency band of the exciter was set from 5 Hz to 250 Hz, and the BEHs were tested under four different excitation levels, which were 0.06, 0.12, 0.20 and 0.28 $(m/s^2)^2/Hz$. An oscilloscope MSOX3052A was applied to record the experimental data from the piezoelectric elements.

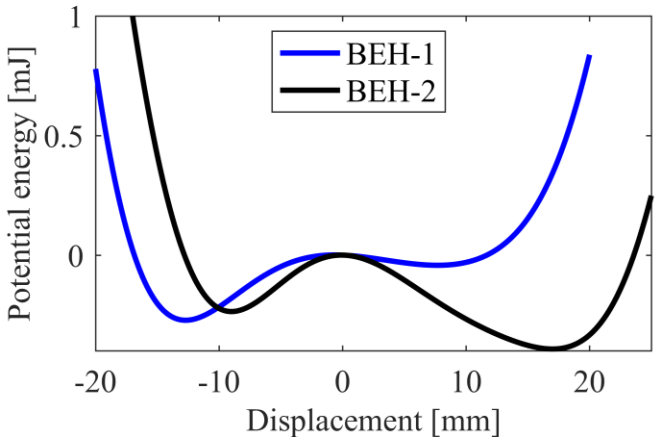

Fig. 13. Experimental potential energy function of BEH-1 and BEH-2 (BEH-2 and BEH-3)

Figure 14 (a) shows the voltage response of BEH-1 with an excitation intensity of 0.06 $(m/s^2)^2/Hz$. BEH-1 was ablw to occasionally oscillate across the potential barrier and the maximum output voltage reaches 11 V. From the frequency spectrum for this case, shown in Fig. 15 (a), it is seen that the response frequency is mainly distributed around 60 Hz, while there is also a distribution range around 20 Hz. When the excitation intensity is increased to 0.12 $(m/s^2)^2/Hz$, the voltage response in Fig. 14 (b) indicates that inter-well motion appeared more frequently and a larger output was generated. Figure 15 (b) shows the corresponding frequency spectrum and in this condition the frequency range from 20 Hz to 30 Hz is a main area for the distribution. As the excitation intensity is further increased to 0.20 and 0.28 $(m/s^2)^2/Hz$, BEH-1 was able to travel across the potential barrier more easily, thus achieving a larger output electrical power of X and Y respectively. In particular, the amplitude in the frequency spectrum for the intensity of 0.28 $(m/s^2)^2/Hz$ shows a clear increasing

trend when compared with a lower excitation level.

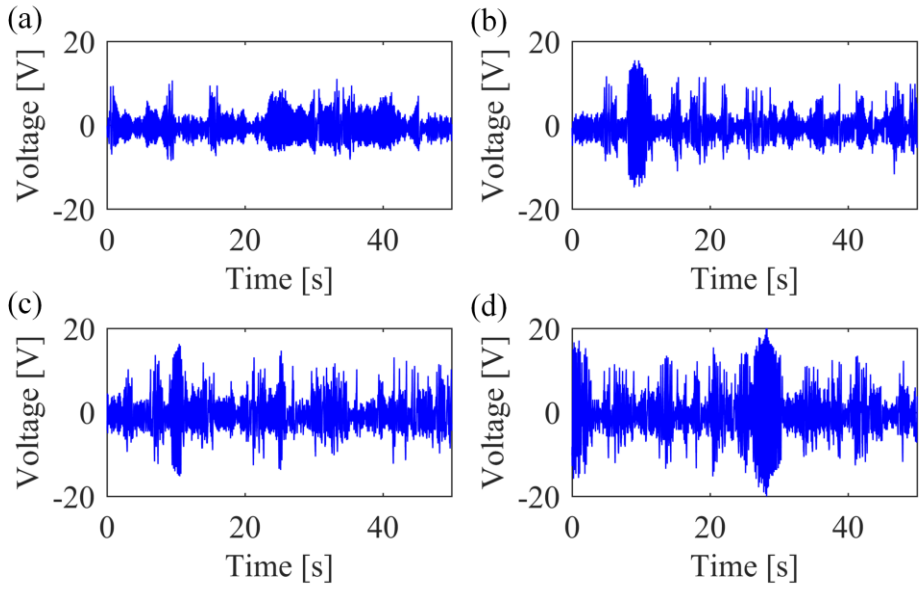

Fig. 14. Experiment voltage response of BEH-1 under different excitation intensity: (a) D=0.06 $(m/s^2)^2/Hz$; (b) D=0.12 $(m/s^2)^2/Hz$; (c) D=0.20 $(m/s^2)^2/Hz$; (d) D=0.28 $(m/s^2)^2/Hz$.

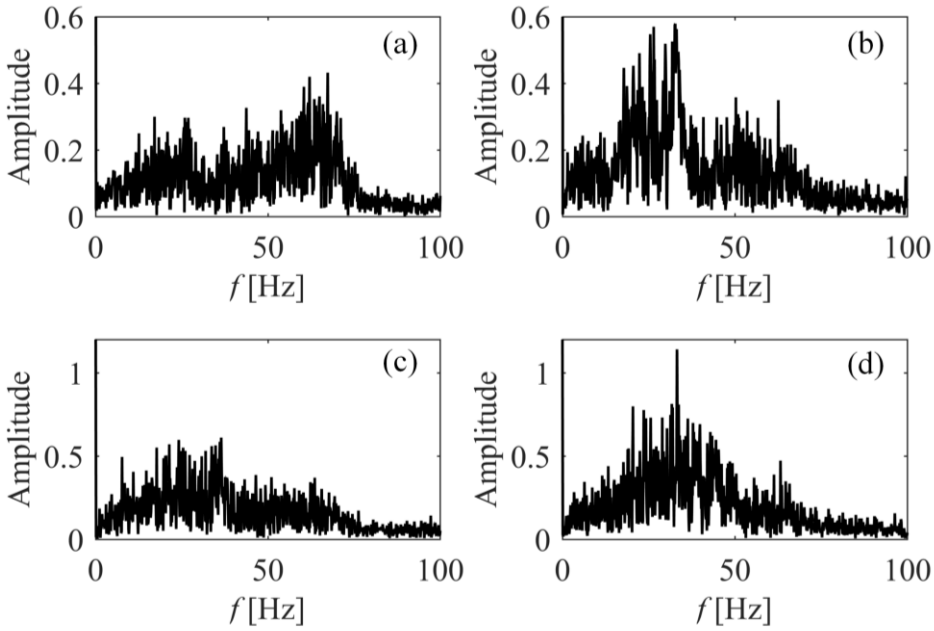

Fig. 15. Experimental frequency spectrum of BEH-1 under different excitation intensity: (a) D=0.06 $(m/s^2)^2/Hz$; (b) D=0.12 $(m/s^2)^2/Hz$; (c) D=0.20 $(m/s^2)^2/Hz$; (d) D=0.28 $(m/s^2)^2/Hz$.

To compare the performance of BEH-1 and BEH-2, their average output powers under different excitation intensities are plotted in Fig. 16. When the excitation intensity was 0.06 $(m/s^2)^2/Hz$, the

average output power of BEH-1 and BEH-2 are 0.78 μW and 0.52 μW respectively. As the excitation intensity increases, the average output power show an increasing trend and the maximum output power of BEH-1 and BEH-2 reaches 2.65 μW and 1.95 μW respectively under an excitation intensity of 0.28 $(m/s^2)^2/Hz$. In general, an increase of the excitation intensity will positively contribute to electrical output power, and the BEH with shallower potential wells will generate a larger output power under a certain excitation level.

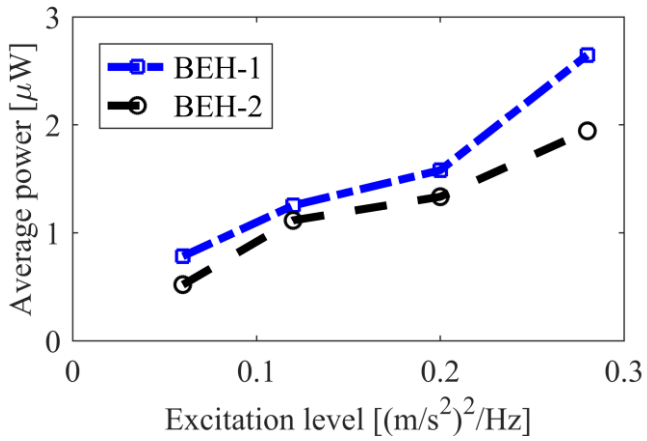

Fig. 16. Experimental average output power of BEH-1 and BEH-2 under different excitation intensity.

5. Conclusion

This paper investigates the influence of asymmetric potentials on the output and response probability of bistable energy harvesters (BEHs) under Gaussian white noise excitations. The presence of asymmetries in BEHs will result in potential functions with different well depth, and the influence of potential well depth on the harvester response is firstly considered based on the output and probability density function (PDF) of displacement. Numerical simulations indicate that an increase of potential well depth will make BEHs have a smaller probability to vibrate across the potential barrier under low excitation levels, thus generating lower electrical energy. However, under a larger excitation intensity, the output will increase with an increase in the potential well depth since

the distance between the two wells becomes the main factor determining the output on this occasion. When asymmetries appear in the potential function of BEHs, we demonstate that it has a negative influence on the electrical output under a low excitation intensity and the negative effect will increase with the degree of asymmetry. However, under larger excitation levels, the influence on the electrical output is small. From our probability analysis, PDFs of displacement demonstrate that the appearance of asymmetry makes the system have a larger probability to oscillate in the deeper potential well and result in an asymmetric bimodal distribution of the PDFs. An increase of degree of asymmetry will increase the negative effect while an increase in the excitation intensity will reduce it. In the experiments, two asymmetric potential BEHs are created and excited under different levels of excitation intensity. Measurements of average output power validates that an increase of the excitation level contributes positively to the output power, while an increase in the asymmetric degree and potential well depth has an opposite effect. As a result, the materials and manufacturing methods employed for the creation of bistable energy harvesters should attempt to optimize the symmetry of the potential functions to maxmise broadband performance.

Acknowledgment

This study was supported by the National Natural Science Foundation of China (Grant No. 51575426, 51811530321); this research was partly supported by China Scholarship Council.

References

1. P. D. Mitcheson, E. M. Yeatman, G. K. Rao, A. S. Holmes, T. C. Green, Proceedings of the IEEE **96**, 1457 (2008).
2. S. P. Pellegrini, N. Tolou, M. Schenk, J. L. Herder, Journal of Intelligent Material Systems and Structures **24**, 1303 (2012).
3. M. F. Daqaq, R. Masana, A. Erturk, D. Dane Quinn, Applied Mechanics Reviews **66**, 040801 (2014).
4. J. Siang, M. H. Lim, M. Salman Leong, Int J Energ Res **42**, 1866 (2018).
5. P. L. Green, E. Papatheou, N. D. Sims, Journal of Intelligent Material Systems and Structures **24**, 1494 (2013).
6. S. Siddiqui, D.-I. Kim, E. Roh, L. T. Duy, T. Q. Trung, M. T. Nguyen, N.-E. Lee, Nano Energy **30**, 434 (2016).
7. M. Lee, C. Y. Chen, S. Wang, S. N. Cha, Y. J. Park, J. M. Kim, L. J. Chou, Z. L. Wang, Advanced materials **24**, 1759 (2012).
8. A. Almusallam, Z. Luo, A. Komolafe, K. Yang, A. Robinson, R. Torah, S. Beeby, Nano Energy **33**, 146 (2017).
9. M. Salauddin, M. S. Rasel, J. W. Kim, J. Y. Park, Energy Conversion and Management **153**, 1 (2017).
10. T. Quan, Y. Wu, Y. Yang, Nano Research **8**, 3272 (2015).
11. M.-K. Kim, M.-S. Kim, S. Lee, C. Kim, Y.-J. Kim, Smart Mater Struct **23**, 105002 (2014).
12. I. Iyyappan, M. Ponmurugan, Journal of Statistical Mechanics: Theory and Experiment **2017**, 093207 (2017).
13. R. L. Harne;, K. W. Wang, (2018).
14. S. Zhou, J. Cao, W. Wang, S. Liu, J. Lin, Smart Mater Struct **24**, 055008 (2015).
15. S. Roundy, P. K. Wright, J. Rabaey, Comput Commun **26**, 1131 (2003).
16. M. F. Daqaq, Journal of Sound and Vibration **330**, 2554 (2011).
17. M. F. Daqaq, Nonlinear Dynamics **69**, 1063 (2012).
18. Y. Zhu, J. W. Zu, Applied Physics Letters **103**, 041905 (2013).
19. S. Zhou, J. Cao, D. J. Inman, S. Liu, W. Wang, J. Lin, Applied Physics Letters **106**, 093901 (2015).
20. Y. Zhang, C. S. Cai, W. Zhang, Smart Mater Struct **23**, 055002 (2014).
21. N. Tran, M. H. Ghayesh, M. Arjomandi, International Journal of Engineering Science **127**, 162 (2018).
22. Y. Zhang, L. Tang, K. Liu, Journal of Intelligent Material Systems and Structures **28**, 307 (2016).
23. H.-C. Song, P. Kumar, R. Sriramdas, H. Lee, N. Sharpes, M.-G. Kang, D. Maurya, M. Sanghadasa, H.-W. Kang, J. Ryu, W. T. Reynolds, and S. Priya, Appl Energ **225**, 1132 (2018).
24. K. Q. Fan, Q. X. Tan, H. Y. Liu, Y. W. Zhang, M. L. Cai, Mech Syst Signal Pr **117**, 594 (2019).
25. A. Erturk, J. Hoffmann, D. J. Inman, Applied Physics Letters **94**, 254102 (2009).
26. S. Zhao, A. Erturk, Applied Physics Letters **102**, 103902 (2013).
27. R. Masana, M. F. Daqaq, Journal of Vibration and Acoustics **133**, 011007 (2011).
28. A. F. Arrieta, T. Delpero, A. E. Bergamini, P. Ermanni, Applied Physics Letters **102**, 173904 (2013).
29. S. Zhou, J. Cao, A. Erturk, J. Lin, Applied Physics Letters **102**, 173901 (2013).
30. W. Liu, F. Formosa, A. Badel, Journal of Intelligent Material Systems and Structures **28**, 671 (2016).
31. P. Wolszczak, K. Łygas, G. Litak, Mech Syst Signal Pr **107**, 43 (2018).
32. P. Kim, J. Seok, Journal of Sound and Vibration **333**, 5525 (2014).
33. Z. Zhou, W. Qin, P. Zhu, Mech Syst Signal Pr **84**, 158 (2017).
34. Z. Zhou, W. Qin, Y. Yang, P. Zhu, Sensors and Actuators A: Physical **265**, 297 (2017).
35. G. Litak, M. I. Friswell, S. Adhikari, Applied Physics Letters **96**, 214103 (2010).
36. Y. G. Yang, W. Xu, Nonlinear Dynamics **94**, 639 (2018).
37. W.-A. Jiang, L.-Q. Chen, Journal of Sound and Vibration **377**, 264 (2016).
38. R. Zheng, K. Nakano, H. Hu, D. Su, M. P. Cartmell, Journal of Sound and Vibration **333**, 2568 (2014).

39. H. Li, W. Qin, W. Deng, R. Tian, The European Physical Journal Plus **131**, (2016).
40. Y. Jin, S. Xiao, Y. Zhang, Journal of Statistical Mechanics: Theory and Experiment **2018**, 123211 (2018).
41. C. B. Lan, W. Y. Qin, H. T. Li, Acta Phys Sin-Ch Ed **64**, (2015).
42. H. Li, W. Qin, Nonlinear Dynamics **81**, 1751 (2015).
43. Z. Zhou, W. Qin, P. Zhu, Energy **126**, 527 (2017).
44. R. L. Badzey, P. Mohanty, Nature **437**, 995 (2005).
45. V. N. Chizhevsky, G. Giacomelli, Phys Rev E **73**, 022103 (2006).
46. S. Jeyakumari, V. Chinnathambi, S. Rajasekar, M. A. F. Sanjuan, International Journal of Bifurcation and Chaos **21**, 275 (2011).
47. L. Cveticanin, M. Zukovic, G. Mester, I. Biro, J. Sarosi, Acta Mechanica **227**, 1727 (2016).
48. R. L. Harne, K. W. Wang, Journal of Vibration and Acoustics **136**, 021009 (2013).
49. Q. F. He, M. F. Daqaq, Journal of Sound and Vibration **333**, 3479 (2014).
50. E. Halvorsen, Physical Review E **87**, (2013).
51. W. Wang, J. Cao, C. R. Bowen, Y. Zhang, J. Lin, Nonlinear Dynamics **94**, 1183 (2018).
52. W. Wang, J. Cao, C. R. Bowen, D. J. Inman, J. Lin, Applied Physics Letters **112**, 213903 (2018).
53. S. Zhou, L. Zuo, Commun Nonlinear Sci **61**, 271 (2018).
54. Y. Li, S. Zhou, AIP Advances **8**, 125212 (2018).
55. W. Wang, J. Cao, C. R. Bowen, G. Litak, The European Physical Journal B **91**, (2018).
56. Z. Qiao, Y. Lei, N. Li, Mech Syst Signal Pr **122**, 502 (2019).
57. Y. G. Leng, Z. H. Lai, Acta Phys Sin-Ch Ed **63**, 020502 (2014).